Am J Physiol Regul Integr Comp Physiol 285: R939–R949, 2003.
First published July 10, 2003; 10.1152/ajpregu.00200.2003.

Disrupted circadian rhythms in VIP- and PHI-deficient mice

Christopher S. Colwell, Stephan Michel, Jason Itri, Williams Rodriguez, J. Tam, Vincent Lelievre, Zhou Hu, X. Liu, and James A. Waschek
Mental Retardation Research Center, Department of Psychiatry and Biobehavioral Sciences, University of California, Los Angeles, California 90024-1759

Submitted 15 April 2003; accepted in final form 4 July 2003

Colwell, Christopher S., Stephan Michel, Jason Itri, Williams Rodriguez, J. Tam, Vincent Lelievre, Zhou Hu, X. Liu, and James A. Waschek. Disrupted circadian rhythms in VIP- and PHI-deficient mice. *Am J Physiol Regul Integr Comp Physiol* 285: R939–R949, 2003. First published July 10, 2003; 10.1152/ajpregu.00200.2003.—The related neuropeptides vasoactive intestinal peptide (VIP) and peptide histidine isoleucine (PHI) are expressed at high levels in the neurons of the suprachiasmatic nucleus (SCN), but their function in the regulation of circadian rhythms is unknown. To study the role of these peptides on the circadian system in vivo, a new mouse model was developed in which both VIP and PHI genes were disrupted by homologous recombination. In a light-dark cycle, these mice exhibited diurnal rhythms in activity which were largely indistinguishable from wild-type controls. In constant darkness, the VIP/PHI-deficient mice exhibited pronounced abnormalities in their circadian system. The activity patterns started ~8 h earlier than predicted by the previous light cycle. In addition, lack of VIP/PHI led to a shortened free-running period and a loss of the coherence and precision of the circadian locomotor activity rhythm. In about one-quarter of VIP/PHI mice examined, the wheel-running rhythm became arrhythmic after several weeks in constant darkness. Another striking example of these deficits is seen in the split-activity patterns expressed by the mutant mice when they were exposed to a skeleton photoperiod. In addition, the VIP/PHI-deficient mice exhibited deficits in the response of their circadian system to light. Electrophysiological analysis indicates that VIP enhances inhibitory synaptic transmission within the SCN of wild-type and VIP/PHI-deficient mice. Together, the observations suggest that VIP/PHI peptides are critically involved in both the generation of circadian oscillations as well as the normal synchronization of these rhythms to light.

peptide histidine isoleucine; vasoactive intestinal peptide; suprachiasmatic nucleus; GABA; inhibitory postsynaptic currents

IN MAMMALS, THE PART OF THE nervous system responsible for most circadian behavior can be localized to the suprachiasmatic nucleus (SCN). Although previous studies suggest that each SCN neuron may be an independent oscillator (10), these pacemaker cells must be synchronized to each other as well as to the environment to function adaptively. Therefore, answers to questions about cell-to-cell communication within the SCN lie at the core of understanding how this timing system operates. The daily cycle of light and dark is the dominant environmental cue responsible for synchronizing this biological timing system to the environment. The SCN neurons receive photic information directly from the retinal hypothalamic tract (RHT). The RHT is composed of a distinct subset of retinal ganglion cells that recent studies suggest contain a novel photopigment melanopsin and are directly light sensitive (3, 14). These ganglion cells appear to utilize the neuropeptide pituitary adenylyl cyclase-activating peptide (PACAP) and glutamate as neuromodulators and/or neurotransmitters to communicate with the SCN (e.g., Refs. 8, 10, and 12). Many of the SCN neurons that receive retinal input from these cells are located in the ventrolateral (or core) region of the SCN and express GABA and, in many cases, vasoactive intestinal peptide (VIP) and the peptide histidine isoleucine (PHI; e.g., Refs. 4 and 20). These retino-recipient cells then convey this environmental information to the rest of the SCN.

There is a small but growing body of data suggesting that VIP itself may be an important signaling molecule within the SCN. The concentration of VIP within the SCN can be regulated by light, and a receptor for VIP and PACAP, the $VPAC_2$ receptor, is widely distributed within the SCN (5, 31, 32). In brain slice preparations, application of VIP alters the firing rate of SCN neurons through a $VPAC_2$ receptor-dependent mechanism (9, 26) and induces expression of *mPer1* and *mPer2* genes (22). Functionally, the administration of VIP, and to a lesser extent PHI, can cause phase shifts of the circadian rhythm in vivo and in vitro (2, 25, 27). Mice overexpressing $VPAC_2$ receptors exhibit a shorter free-running period (31), whereas mice deficient in this receptor exhibit profound disruptions in their daily rhythms in wheel-running activity, electrical activity in SCN neurons, and rhythmic gene expression (9, 13). To investigate the functional role of VIP in vivo, a new mouse model was developed in which the VIP and PHI genes were disrupted by targeted mutagenesis. After generation and characterization of these mice, behavioral analysis was utilized to examine the impact of the disruption of these genes on the circadian rhythm of wheel-running activity. Finally, whole cell patch electrophysiological techniques were utilized to determine

Address for reprint requests and other correspondence: C. S. Colwell, Mental Retardation Res. Ctr., Univ. of California - Los Angeles, 760 Westwood Plaza, Los Angeles, CA 90024-1759 (E-mail: ccolwell@mednet.ucla.edu).

The costs of publication of this article were defrayed in part by the payment of page charges. The article must therefore be hereby marked "*advertisement*" in accordance with 18 U.S.C. Section 1734 solely to indicate this fact.

whether VIP and PHI regulate spontaneous inhibitory synaptic currents recorded within SCN neurons.

MATERIALS AND METHODS

Establishment of mice with targeted VIP/PHI gene disruption. In previous work, we cloned and characterized the mouse VIP gene (30, 36, 37). On the basis of this information, a homologous recombination targeting construct was prepared (Fig. 1*A*). This construct contained a 6.2-kb *Pst* I/*Sph* I 5′-portion of the VIP gene, a neomycin resistance cassette (p*PGK* neo bpA) in inverse orientation, a 2.6-kb *Sph* I/*Eco*RI 3′-VIP gene fragment, and a herpes simplex thymidine kinase cassette from pIC19R/MC-1-TK. This construct was introduced into embryonic stem (ES) cells (129/sv agouti, wild-type albino locus) by the University of California Los Angeles (UCLA) transgenic/embryonic stem cell core facility. Three homologous recombinant clones were identified and were injected into blastocysts of C57BL/6 mice, which then were transplanted into the uteri of pseudopregnant foster mothers. Resulting chimeric mice were bred with C57BL/6 females. Germ line transmission from chimeric mice derived from two of these clones was confirmed by Southern analysis of DNA obtained from tail biopsies by use of a probe external to targeting sequences (Fig. 1*B*). After confirmation of germ line transmission, DNA samples were assayed by triple primer PCR with the use of the following primers: omVIPF4+ TTTCAAGGTGTGGGGCTAGAGACATACA (0.5 μM), omVIPF5− TTACCTGATTCGTTTGCCAATGAGTGAC (1.0 μM), and opNEO10− GCCCGGAGATGAGGAAGAGGAGAACAG (0.5 μM). The reaction also contained 0.2 mM dNTPs, 1.0 mM $MgSO_4$, and 1 μl of *Taq* polymerase [5:1 ratio of Titanium *Taq* (Clontech, San Diego, CA) to Native *Pfu* (Stratagene, La Jolla, CA)]. A touchdown PCR procedure was used. After samples were heated to 94°C for 1 min, they were subject to PCR for a total of 35 cycles as follows: denaturation at 94°C for 1 min, annealing for 30 s (starting at 70°C and decreasing by 1 degree each cycle until 60°C, then maintaining at 60°C), and elongation at 72°C for 4.5 min. The reaction was finished with an extra 5-min elongation at 72°C and a 20-min period at 4°C.

Behavioral studies. Behavioral effects were examined using offspring of F1 C57BL/6 × 129/sv VIP +/− mice. Subsequent studies were performed with VIP −/− generated after backcrossing with C57BL/6 mice for six to seven generations. These mice exhibited running-wheel behavior that was not different than that observed on a mixed background. Homozygous VIP/PHI mutant mice and wild-type controls from the same litter were analyzed in most cases, but occasionally, when a wild-type male littermate was unavailable, an age-matched control mouse from another litter of the same background was used. Mice derived from the two different ES clones were found to exhibit similar circadian abnormalities, and so the resulting data were pooled. Control C57BL/6 mice were obtained from breeding colonies maintained at UCLA. In all studies, the recommendations for animal use and welfare, as dictated by the UCLA Division of Laboratory Animals and the guidelines from the National Institutes of Health, were followed.

Male mice, at least 10 wk of age, were housed individually, and their wheel-running activity was recorded as revolutions per 3-min interval. The running wheels and data acquisition system were obtained from Mini Mitter (Bend, OR). The animals were exposed to a 12:12-h light-dark cycle (LD) for 2–3 wk (light intensity 36 $\mu W/cm^2 \cong 120$ lux). The animals were then placed into constant darkness (DD) to assess their free-running activity pattern. Some mice in LD were also exposed to a light treatment (white light, 60 min, 15 $\mu W/cm^2 \cong$ 50 lux) during their activity period to measure negative

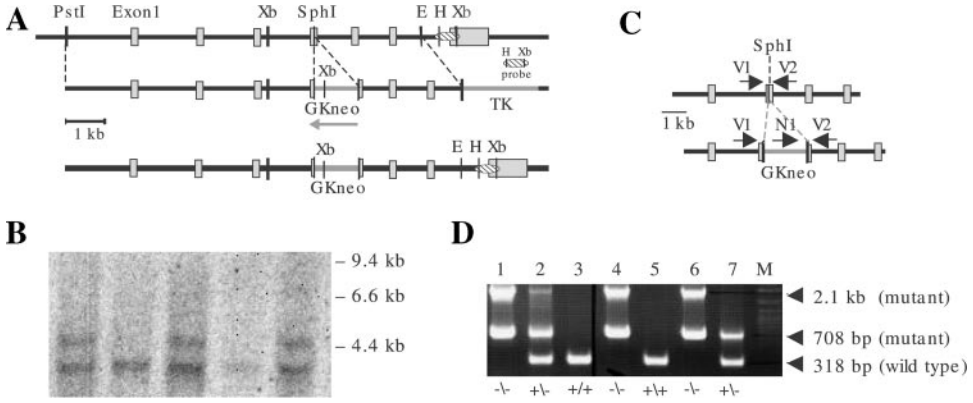

Fig. 1. Vasoactive intestinal peptide (VIP)/peptide histidine isoleucine (PHI) gene-disruption strategy and confirmation of the targeted mutation in mice. *A*: gene-disruption strategy. *Top* segment is the normal VIP gene, with all 7 exons indicated by boxes. In the targeting construct (*middle*), the neomycin cassette was placed in inverse orientation just upstream from the PHI-encoding sequences on exon 4. VIP is encoded on exon 5. *Bottom* segment represents the desired gene structure altered by homologous recombination. Xb, *Xba*I; E, *Eco*RI; H, *Hind* III; GKneo, p*PGK* neo bpA; TK, pIC19R/MC-1-TK. *B*: confirmation of VIP gene disruption in offspring of a chimeric mouse. Tail DNA from 5 offspring was digested with *Xba*I and analyzed by Southern blot. Blot was probed with the 600-bp *Hind* III/*Xba*I gene fragment indicated in *A*. *Lanes 1*, *3*, and *5* are heterozygous for the disrupted gene because they contain bands at the predicted sizes for the endogenous and mutated genes (3.9 and 4.4 kb, respectively). *Lanes 2* and *4* were wild type. *C* and *D*: PCR analysis of a litter of offspring from 2 mice heterozygous for a targeted mutation in the VIP gene. Relevant portions of the wild-type (*top*) and disrupted VIP (*bottom*) genes are shown in *C*. Points of arrows indicate the positions of the 3 primers used in the PCR reaction. *D*: an ethidium-stain agarose gel of reaction products from 7 offspring alongside a size marker (M). As indicated on the *right*, the mutant allele gives 2 bands. The 2.1-kb band is generated by primers V1 and V2. The 708-bp band is generated by primers N1 and V2. The wild-type allele gives a product of 318 bp, generated by V1 and V2. In heterozygous mice, the 2.1-kb band is sometimes faint (for example *mouse 7*), because the 2.1-kb and 318-bp bands both require primer V2, and the 318-bp band amplifies more efficiently.

masking behavior, i.e., light-induced suppression of activity. Other mice in LD or constant light (LL) were exposed to a dark treatment (no light, 60 min) to measure positive masking behavior. In each case, the number of revolutions during this light treatment was compared with the number recorded during the same phase on the previous day in the dark (21). Stimulus intensity (irradiance) was measured with a radiometer (United Detector Technologies, Hawthorne, CA). All handling of animals was carried out either in the light portion of the LD cycle or in DD with the aid of an infrared viewer (FJW Industries).

The locomotor activity rhythms of mice were analyzed by periodogram analysis combined with a χ^2 test with 0.1% significance level (El Temps, Barcelona, Spain) on the raw data. The periodogram shows the amplitude (=power) of periodicities in the time series for all periods of interest (between 20 and 31 h in 3-min steps). From the variable *Qp* obtained from the periodogram, the percentage of variance explained by the rhythm is $Qp \times 100/n$. With n being the data number, the *Qp* value is then normalized (e.g., 6). During DD, we found that a power value of >30% indicated a strong and coherent activity rhythm. Power values <30% were consistent with a weaker expression of one single period of the activity rhythm and indicated a less coherent activity pattern. Slopes of an eye-fitted line through the onsets were also used to confirm period estimates made with the periodogram analysis. To estimate the cycle-to-cycle variability in activity onset, a linear regression to 15 cycles of onset of activity was calculated. The onset of activity for each cycle was defined as the phase at which the activity levels of the animal first equaled the mean activity level for that cycle. The divergence between the measured and predicted onsets was then determined, and the average difference was calculated for each animal. We found that using the mean activity level as a threshold provided a very simple and reliable measure for the detection of the start of an activity bout. The duration of each cycle devoted to running-wheel activity is designated alpha (α), and the duration of non-wheel-running activity is designated rho (ρ). To measure these parameters, the average pattern of activity (i.e., the form estimate) was determined at moduloperiod for each animal in DD for 15 cycles. Then for each waveform, α was calculated as the time during which the motor activity was above the medium.

Brain slice preparation. Brain slices were prepared using standard techniques from mice (C57BL/6) between 21 and 48 days of age. Mice were killed by decapitation, and brains were dissected and placed in cold oxygenated artificial cerebral spinal fluid (ACSF) containing (in mM) NaCl 130, $NaHCO_3$ 26, KCl 3, $MgCl_2$ 5, NaH_2PO_4 1.25, $CaCl_2$ 1, and glucose 10 (pH 7.2–7.4; osmolality 290–300 mosmol/kgH_2O). After slices were cut, transverse sections (350 μm) were placed in ACSF (25–27°C) for at least 1 h (in this solution, $CaCl_2$ was increased to 2 mM and $MgCl_2$ was decreased to 2 mM). Slices were constantly oxygenated with 95%O_2-5% CO_2. Slices were placed in a perfusion chamber (Warner Instruments, Hamden, CT) attached to the stage of the fixed-stage upright microscope. The slice was held down with thin nylon threads glued to a platinum wire and submerged in continuously flowing, oxygenated ACSF at 2 ml/min. Solution exchanges within the slice were achieved by a rapid gravity feed delivery system. In our system, the effects of bath-applied drugs begin within 15 s and are typically complete by 1–2 min.

Infrared differential interference contrast videomicroscopy. Slices were viewed with an upright compound microscope (Olympus BX50), using a water immersion lens (40×) and differential interference contrast optics. They were illuminated with near infrared (IR) light by placement of an IR bandpass filter (750–1,050 nm) in the light path. The image was detected with an IR-sensitive video camera (Hamamatsu C2400, Bridgewater, NJ) and displayed on a video monitor. A camera controller allowed analog contrast enhancement and gain control. Cells were typically visualized from 30–100 μm below the surface of the slice. In the present study, IR videomicroscopy was utilized to visualize cells within the brain slice and to limit some of the uncertainty as to the cell type. This imaging technique allowed us to clearly see the SCN and to exclude cells from the surrounding hypothalamic regions.

Whole cell patch-clamp electrophysiology. Methods were similar to those described previously (8, 19). Briefly, electrodes were pulled on a multistage puller (Sutter P-97, Novato, CA). Electrode resistance in the bath was typically 3–6 MΩ. The standard solution in the patch pipette contains (in mM) K-gluconate 112.5, HEPES 10, MgATP 5, NaCl 4, EGTA 1, $MgCl_2$ 1, $CaCl_2$ 0.5, GTP-Tris 1, leupeptin 0.1, and phosphocreatine 10. The pH was adjusted to 7.25–7.3 by use of KOH and the osmolality to 290–295 mosmol/kgH_2O by use of sucrose. Whole cell recordings were obtained with an Axon Instruments 200B amplifier and monitored online with pCLAMP (Axon Instruments, Foster City, CA). Because of the composition of the pipette filling solution, the calculated reversal potential for the GABA currents was −46 mV, and therefore inhibitory postsynaptic currents (IPSCs) appeared as inward currents at the holding potential of −70 mV. To minimize changes in offset potentials, the ground path used a KCl agar bridge. Cells were approached with slight positive pressure (2–3 cmH_2O), and offset potentials were corrected. The pipette was lowered to the vicinity of the membrane keeping a positive pressure. After forming a high-resistance seal (2–10 GΩ) by applying negative pressure, a second pulse of negative pressure was used to break the membrane. While entering the whole cell mode, a repetitive test pulse of 10 mV was delivered in a passive potential range (≈−60 to −70 mV). Whole cell capacitance and electrode resistance were neutralized and compensated (50–80%) by use of the test pulse. Data acquisition was then initiated. Series and input resistance was monitored repeatedly by checking the response to small pulses in a passive potential range. Series resistance was not compensated, and the maximal voltage error due to this resistance was calculated to be 6 mV. The access resistance of these cells ranged from 15 to 35 MΩ, and the cell capacitance was typically between 6 and 18 pF.

Under voltage-clamp [membrane potential (V_m) = −70 mV], the holding current was monitored throughout the experiment. Spontaneous postsynaptic currents were analyzed using the MiniAnalysis program (Synaptosoft, Decatur, GA). The software was used to automatically record the number and peak amplitude of spontaneous IPSCs (sIPSCs) recorded in gap-free mode of pCLAMP software. Each automatically detected event was then manually checked to ensure that the baseline and peak were accurately determined. The mean frequency, amplitude, rise time, and decay time of the IPSCs were then calculated for each neuron during 60- to 360-s sampling periods.

Immunocytochemistry. Control and mutant mice were anesthetized and perfused with phosphate-buffered saline (PBS) followed by 4% paraformaldehyde in PBS. Brains were dissected, postfixed at 4°C overnight, and cryoprotected in 30% sucrose in PBS. Immunocytochemistry was performed simultaneously on free-floating 25-μm cryostat coronal brain sections of wild-type and VIP/PHI −/− mice. Sections were washed for 10 min with PBS and then incubated in 2% H_2O_2 in PBS for 1–2 h. Sections were then washed again in PBS,

dipped in 2% normal goat serum in PBS for 2 h, and then incubated with a 1:1,000 dilution of rabbit anti-VIP-antiserum (Chemicon, raised against synthetic VIP 18–28, catalog no. AB982, Temecala, CA) or a 1:4,000 dilution of rabbit anti-PHI-antiserum (Phoenix Pharmaceuticals, raised against porcine PHI-27, catalog no. H-064-01, Belmont, CA) in PBS at 4°C for 2–3 days. Sections were then washed again in PBS and incubated with biotinylated goat anti-rabbit antibody (1:2,000) for 2 h. Sections were washed again for 10 min in PBS and dipped in an avotin-biotin (Vector ABC kit, Burlingame, CA) solution for 2 h, washed again in PBS, and then placed in filtered 0.05% 3,3′-diaminobenzidine in PBS containing a 1:10,000 dilution of 30% H_2O_2. After sufficient color reaction, sections were washed with PBS and mounted on slides immediately. Sections were then dried overnight, washed with PBS for 10 min, dehydrated with ascending concentrations of ethanol, and coverslipped. Images were captured with SPOT camera systems (Diagnostic Instruments, Sterling Heights, Michigan).

Statistical analyses. Between-group differences were evaluated using *t*-tests or Mann-Whitney rank sum tests when appropriate. Values were considered significantly different if $P < 0.05$. All tests were performed using SigmaStat (SPSS, Chicago, IL). In the text, values are shown as means ± SE.

RESULTS

Generation and characterization of VIP/PHI-deficient mice. To better understand the role of VIP and PHI in vivo, the genes encoding these peptides were disrupted by insertion of a gene encoding a selection marker (neomycin cassette) into exon 4 in a reverse orientation upstream from sequences encoding VIP and PHI, on the fifth and fourth exons, respectively (Fig. 1*A*). In addition, a Herpes simplex thymidine kinase gene was placed at the 3′-end to enable both positive and negative antibiotic selection. This construct was introduced into ES cells. Southern blot analysis revealed the occurrence of successful recombination events in three ES cell clones and germ line transmission from two of these clones (representative analysis showing germ line transmission is shown in Fig. 1*B*). Subsequently, a PCR strategy was developed to identify wild-type, heterozygous, and null VIP/PHI gene mutants generated from heterozygous crosses (Fig. 1, *C* and *D*). Genotyping at 6–8 wk of age indicated that the VIP/PHI mutation followed a normal Mendelian pattern of inheritance that indicates a lack of significant embryonic lethality associated with the mutation. Moreover, both male and female mice homozygous for the targeted mutation were found to be fertile and showed no signs of increased morbidity. Immunohistochemistry confirmed a loss of VIP and PHI expression in mice homozygous for the mutation (Fig. 2).

Behavioral analysis of wheel-running activity in LD and DD. To determine the effect of these genetic manipulations on the circadian system, behavioral analysis of the circadian rhythm in wheel-running activity was carried out with the use of mice (VIP/PHI +/+, VIP/PHI +/−, VIP/PHI −/−) on a mixed C57BL/6 × 129/sv background (Fig. 3). In these experiments, the mice were individually housed in cages containing a running wheel, and their daily activity was recorded. The animals were first synchronized for 2–3 wk to an LD cycle (12:12-h). Under these conditions, all groups appeared to synchronize to the LD cycle and exhibited diurnal rhythms in activity. There was no between-group difference in the phase of activity onset or in

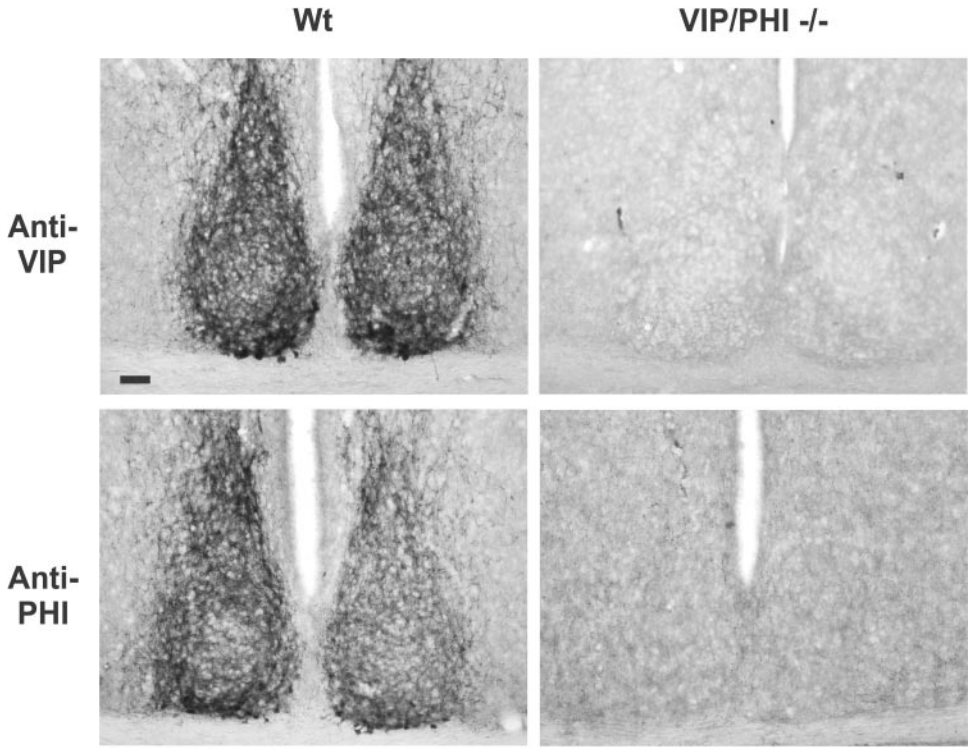

Fig. 2. Photomicrographs illustrate immunoreactive neurons and fibers in the hypothalamic suprachiasmatic nucleus (SCN) of wild-type (Wt; *left*) and VIP/PHI −/− mice (*right*). No VIP- or PHI-immunoreactive cells were observed in the SCN of VIP/PHI −/− mice. Alternative sections were collected and processed in parallel through immunocytochemical procedures. Scale bar = 50 μm.

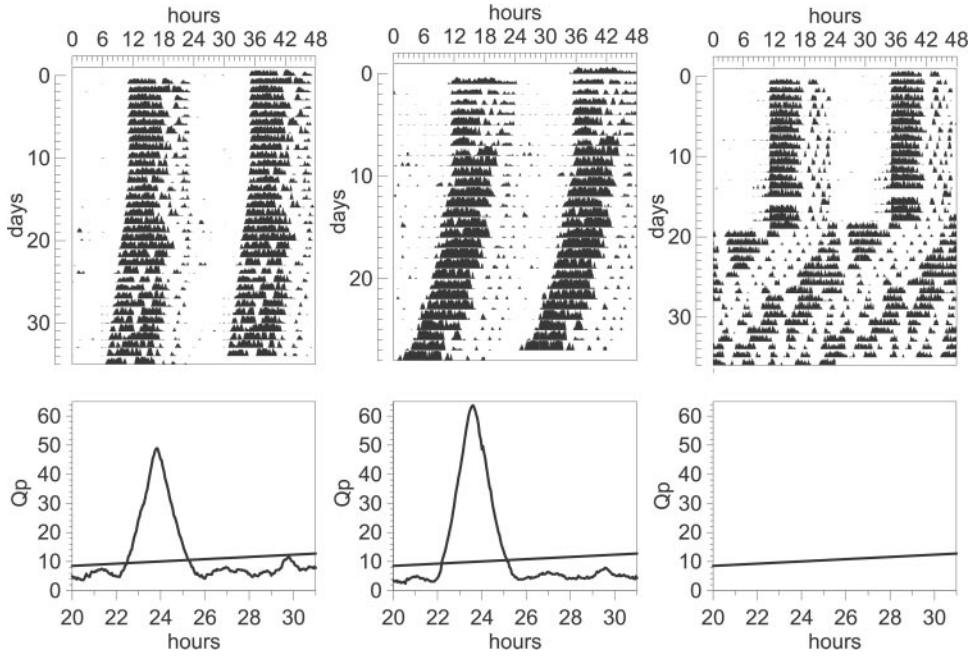

Fig. 3. Examples of wheel-running activity records from VIP/PHI +/+, VIP/PHI +/−, and VIP/PHI −/−mice. Animals were initially entrained to 12:12-h light-dark (LD) cycle and then maintained in constant darkness (DD). Each horizontal row represents the activity record for a 24-h day that is then double plotted. Successive days are plotted from *top* to *bottom*. Gray shaded area represents darkness. *Bottom*: plot of power (expressed as %variance) as a function of period for the activity records of animals in DD. The higher the power, the more robust the behavioral rhythm expressed at that period. *Left*: activity record of a control VIP/PHI +/+ littermate. *Middle*: activity record from a VIP/PHI +/− animal with a relatively coherent activity record. *Right*: activity record from a VIP/PHI −/− animal. Solid lines represent 0.1% significance level. *Qp*, variable obtained from periodogram (see MATERIALS AND METHODS).

cycle-to-cycle variability in activity onset. Overall mean wheel-running activity levels were significantly reduced in the VIP/PHI −/− animals, but the distribution of activity into day or night was similar between groups (Table 1).

Mice were then placed into DD, and their free-running rhythm was recorded. Under these conditions, several striking differences emerged between the VIP/PHI −/−, VIP/PHI +/−, and VIP/PHI +/+ mice in DD (Table 1). First, a few (3/23) of the VIP/PHI −/− animals immediately exhibited an activity pattern that was arrhythmic on a circadian time scale. The remainder of the VIP/PHI −/− mice (20/23) exhibited a circadian rhythm of wheel-running activity with a period that was significantly shorter (22.5 ± 0.1 h; $n = 20$, $P < 0.05$) than littermate controls (23.6 ± 0.1 h, $n = 17$). Periodogram analysis (see Fig. 3, *bottom*) revealed that the circadian rhythm of some of these VIP/PHI −/− mice expressing a short period also showed a second component with a longer period (29.0 ± 0.4 h; $n = 7$). The wheel-running activity of three additional mice decayed into arrhythmicity over the course of several weeks in DD so that by the end of our analysis about one-quarter (6/23) of the VIP/PHI −/− mice were classified as arrhythmic. For the VIP/PHI +/− mice, only one out of nine mice examined became arrhythmic by the 9th wk in DD. Second, once released into DD, the activity of VIP/PHI −/− mice did not start from the phase predicted from the prior LD cycle. Typically, nocturnal rodents will start their activity from a phase close to the onset of darkness in the prior LD (12:12-h) cycle. For example, in the littermate (VIP/PHI +/+) controls, activity began within minutes of the prior lights-off (Table 1). In contrast, the VIP/PHI +/− activity began within 30 min of the prior lights-off, whereas the activity onsets of VIP/PHI −/− animals were clustered around a phase ~8 h earlier (Table 1). This suggests that the animals were synchronized to the LD cycle with an extremely altered phase angle of entrainment (ψ), and the observed activity onset in LD was due to a masking effect of light rather than activity controlled by the circadian pacemaker. Third, the cycle-to-cycle variability in the onset of the daily activity bout was greatly increased in the mutant animals. Normally, the onset of locomotor activity patterns is under precise control of the circadian system. This did not appear to be the case in VIP/PHI −/− animals. Indeed, an analysis of the first 15 cycles in DD indicates that the cycle-to-cycle variability in the phase of activity onset was fourfold higher in VIP/PHI −/− animals compared with controls (Table 1). The VIP/PHI +/− animals exhibited a small but significant increase in variability. Fourth, the VIP/PHI −/− mice exhibited an expansion of the duration of their daily activity bout. Again, focusing our analysis on the first

Table 1. *Comparison of parameters of circadian rhythm in wheel-running behavior for VIP/PHI +/+, VIP/PHI +/−, and VIP/PHI −/− mice*

	Genotype of VIP/PHI Mice		
	+/+	+/−	−/−
Tau, h	23.58 ± 0.07	23.44 ± 0.15	22.55 ± 0.1*†
Power, %variation	46.03 ± 2.86	42.12 ± 3.76	16.81 ± 1.8*†
LD activity, rev/h	289 ± 13	277 ± 10	162 ± 10*†
Phase angle ψ, h	0.004 ± 0.04	0.25 ± 0.08*	8.4 ± 0.47*†
DD activity, rev/h	352 ± 19	410 ± 36	209 ± 30*†
Precision, min	18.5 ± 1.2	23.6 ± 2.1*	77.7 ± 6.1*†
α/ρ Ratio	0.72 ± 0.04	1.02 ± 0.17*	1.25 ± 0.09*
Activity, %	91.7 ± 0.77	93.5 ± 1.1	86.9 ± 1.3*†

Values are means ± SE; $n = 17$ for +/+, $n = 9$ for +/−, and $n = 20$ for −/−. LD, light-dark cycle; DD, constant darkness; rev, revolutions; VIP, vasoactive intestinal peptide; PHI, peptide histidine isoleucine. *Significant difference between control and +/− or −/− mice. †Significant difference between +/− and −/− mice.

15 cycles in DD, the ratio of activity to rest (α/ρ) in VIP/PHI −/− mice was significantly higher compared with the controls (Table 1). These differences in the coherence, α/ρ, and cycle-to-cycle variability in the activity rhythms were also reflected in the significant reduction in the amplitude or power of periodicity in the time series analysis of the activity rhythms expressed by the homozygote mutant animals (Table 1).

Masking. Because the VIP/PHI-deficient mice seem to behave normally under LD but not DD conditions, we next examined the direct influence of light on locomotor activity in these mice. When mice were maintained in an LD cycle, we found no differences in the ability of light [white light, 1 h, zeitgeber time (ZT) 15] to acutely suppress (negative masking) wheel-running activity during an animal's activity period (VIP/PHI +/+: 94 ± 1% suppression, $n = 6$; VIP/PHI −/−: 95 ± 3% suppression, $n = 6$). Next, the ability of dark exposure to increase activity in mice (positive masking) was examined. When mice were exposed to 1 h of dark in the middle of the light portion of an LD cycle (ZT 7), activity was dramatically increased in VIP/PHI −/− [863 ± 300 revolutions (rev)/h, $n = 6$] but not VIP/PHI +/+ littermate controls (34 ± 15 rev/h, $n = 5$). Untreated mice of either genotype are inactive at this phase in their daily cycle. To further explore this dark-evoked response, mice were maintained in constant light (LL) and exposed to 1 h of dark every 4 h throughout a 24-h period (ZT 1, 5, 9, 13, 17, and 21). Because the amount of wheel-running activity in LL conditions was severely reduced, we used the prior LD cycle to determine the phase of the dark pulses. For mice in LL, these dark exposures always caused a dramatic activity increase. For example, wild-type mice exposed to dark (1 h, ZT 17, $n = 8$) showed mean activity levels of 935 ± 267 rev/h compared with 721 ± 132 rev/h for VIP/PHI −/− mice ($n = 8$). Neither genotype exhibited much activity at the same phase in the preceding cycle in LL (VIP/PHI +/+: 65 ± 44 rev/h; VIP/PHI −/−: 103 ± 98 rev/h). Overall, the magnitude of dark-evoked activity did not significantly vary with the time that the treatment was applied or between the wild-type and VIP/PHI-deficient mice. These observations indicate that the loss of the peptides did not alter the negative or positive masking effects of light on locomotor activity.

Skeleton photoperiods. Some of the animals in DD were exposed to a skeleton photoperiod consisting of one or two light pulses per 24-h cycle. The mice exposed to 1:23-h LD synchronized to this light pulse with a single activity bout (Fig. 4). The VIP/PHI −/− mice exhibited an abnormal ψ, as the activity onsets of these animals started ~6 h before the light pulse (5.8 ± 0.7 h, $n = 7$; $P < 0.001$). In contrast, in the littermate (VIP/PHI +/+) controls, activity began around 30 min before lights on (0.45 ± 0.2 h, $n = 7$). The duration of the activity bout was also expanded in the VIP/PHI −/− mice (13.1 ± 0.6 vs. 8.8 ± 1.0 h; $P < 0.005$). The

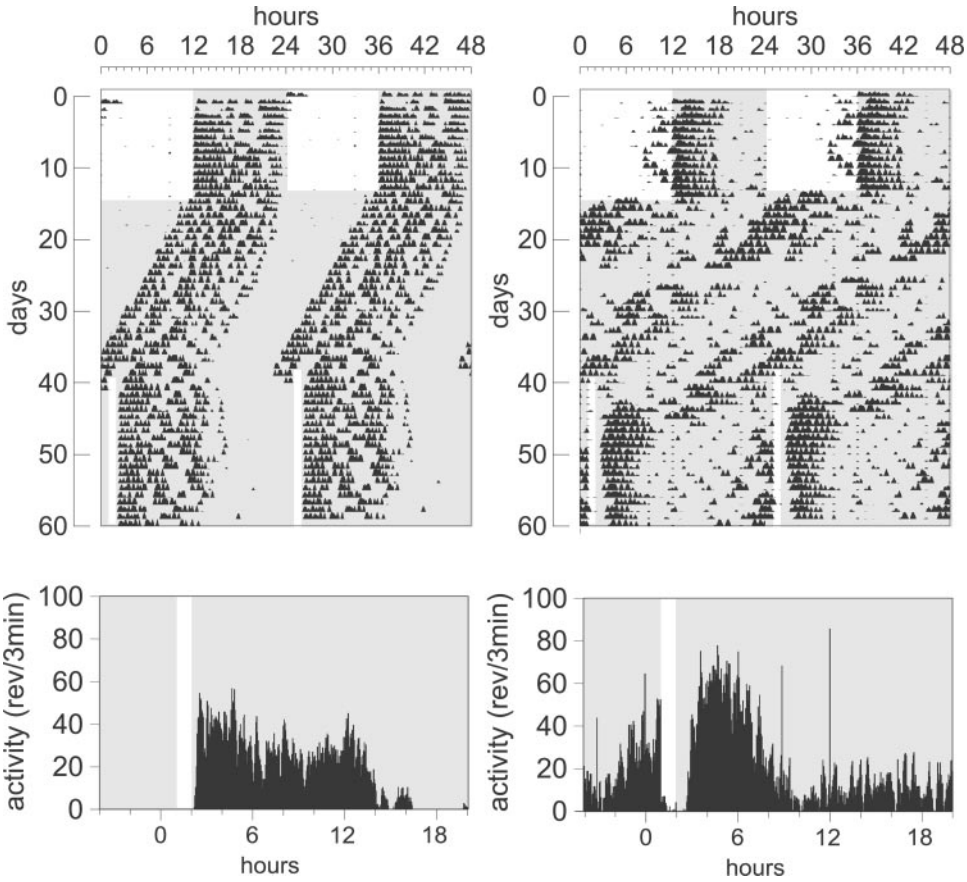

Fig. 4. Examples of wheel-running activity records from VIP/PHI +/+ and −/−mice. Animals were initially entrained to LD cycle (12:12-h), then maintained in DD, and finally placed into a skeleton photoperiod (1:23-h LD). Each horizontal row represents the activity record for a 24-h day that is then double plotted. Successive days are plotted from *top* to *bottom*. Gray shaded area represents darkness. *Left*: activity record of the VIP/PHI +/+ control. *Right*: activity record of a VIP −/− animal. *Bottom*: form estimates, i.e., average distribution of activity measured as running-wheel revolutions (rev) per 3-min bins.

differences between the two genotypes were even more striking when the animals were placed on a skeleton photoperiod consisting of two light pulses per cycle (Fig. 5). When VIP/PHI +/+ mice were exposed to a 1:11:1:11-h LD, the animals synchronized to this skeleton photoperiod with a single activity bout ($\psi = 0.6 \pm 0.3$ h, $\alpha = 9.5 \pm 0.5$ h, 87% of total activity contained in single activity bout, $n = 10$). In contrast, the VIP/PHI −/− animals ($n = 7$) exhibited two major activity bouts, one activity bout after each of the two light pulses. These two activity bouts can be viewed as symmetric with the first pulse capturing ~51% of all activity ($\psi = 7.5 \pm 1.0$ h, $\alpha = 7.0 \pm 0.7$ h) and the second capturing 47% of all recorded activity ($\psi = 8.1 \pm 1.4$ h, $\alpha = 7.0 \pm 0.9$ h).

Light-induced phase shifts. Finally, the effect of the loss of VIP/PHI on phase shifts induced by a single, discrete light treatment was examined. These experiments compared the phase shifts generated by the exposure of a brief light pulse to wild-type (VIP/PHI +/+), heterozygous (VIP/PHI +/−), and homozygous (VIP/PHI −/−) littermates (Fig. 6). Although the VIP/PHI +/+ mice exposed to light at circadian time (CT) 16 (white light, 15 $\mu W/cm^2 \cong 50$ lux, 10 min) showed a 104 ± 13-min ($n = 9$) phase delay, the same treatment in VIP +/− mice caused a 49 ± 6-min phase delay ($n = 11$; $P < 0.01$). The few VIP/PHI −/− that were examined exhibited no significant phase shift in response to this light treatment at CT 16 (16 ± 22 min, $n = 5$). However, instabilities in the activity onset exhibited by these mice (Table 1) made it difficult to accurately assess phase and make interpretation of this experiment difficult.

sIPSCs recorded in SCN are modulated by VIP. Because VIP is coexpressed with GABA, one hypothesis is that VIP modulates inhibitory synaptic transmission within the SCN. To examine this possibility, whole cell voltage-clamp recording techniques were used to measure sIPSCs in SCN neurons visualized by IR-DIC videomicroscopy in a brain slice preparation. For the C57BL/6 mice, the mean frequency and the mean amplitude of sIPSCs recorded from the SCN during the day were 7.0 ± 1.3 events/s (mean ± SE, $n = 7$) and 14.5 ± 1.5 pA, respectively. The time to rise and the time to decay (latency of the inward current peak from the baseline) were 2.6 ± 0.2 and 13 ± 1 ms, respectively. IPSCs were completely abolished with the $GABA_A$ antagonist bicuculline (25 μM, 6 of 6 neurons tested), indicating that they are mediated by $GABA_A$ receptors. In C57BL/6 mice (Fig. 7*A*), VIP (100 nM,

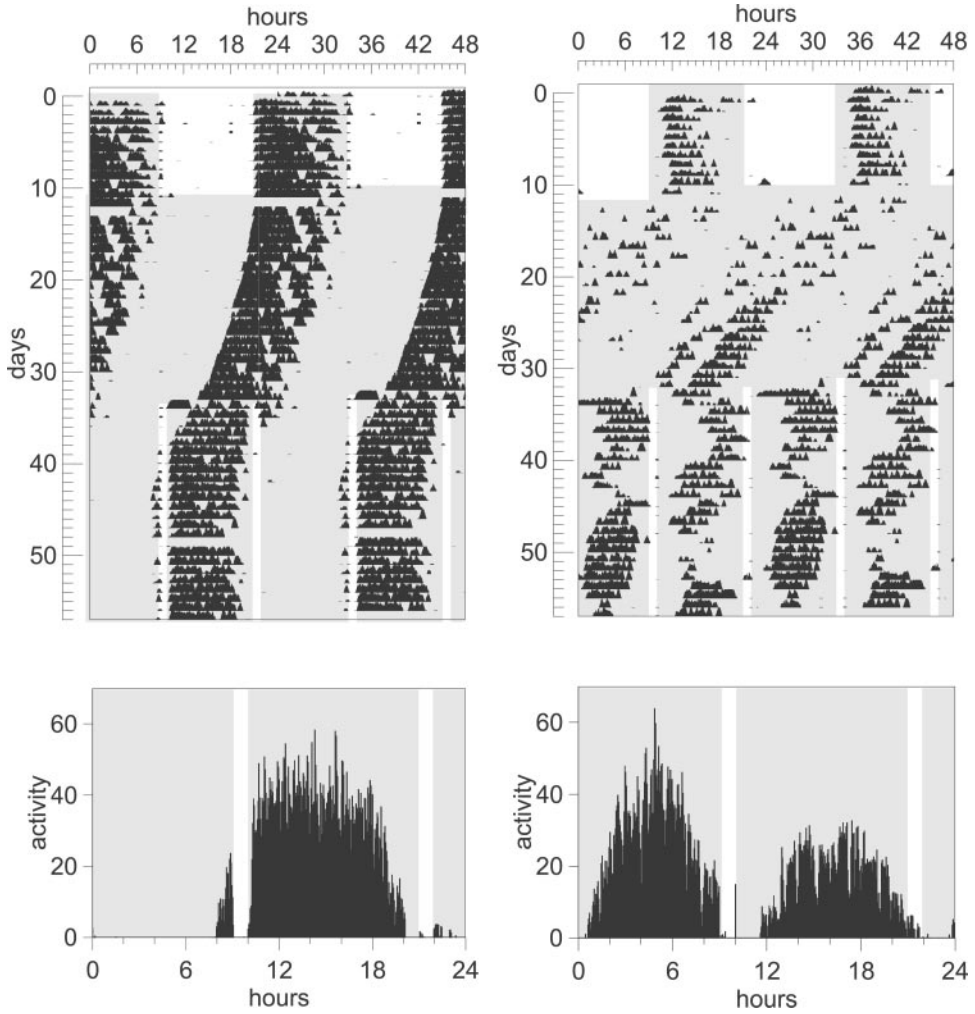

Fig. 5. *Top*: examples of wheel-running activity records from VIP/PHI +/+ and −/− mice. Animals were initially entrained to LD cycle (12:12-h), then maintained in DD, and finally placed into a skeleton photoperiod (1:11:1:11-h LD). Each horizontal row represents the activity record for a 24-h day that is then double plotted. Successive days are plotted from *top* to *bottom*. Gray shaded area represents darkness. *Left*: activity record of the VIP/PHI +/+ control. *Right*: activity record of a VIP/PHI −/− animal. All of the VIP −/− mice exhibited 2 major activity bouts when placed in these lighting conditions, whereas all of the controls exhibited a single activity bout. *Bottom*: form estimates, i.e., average distribution of activity measured as running-wheel revolutions per 3-min bins.

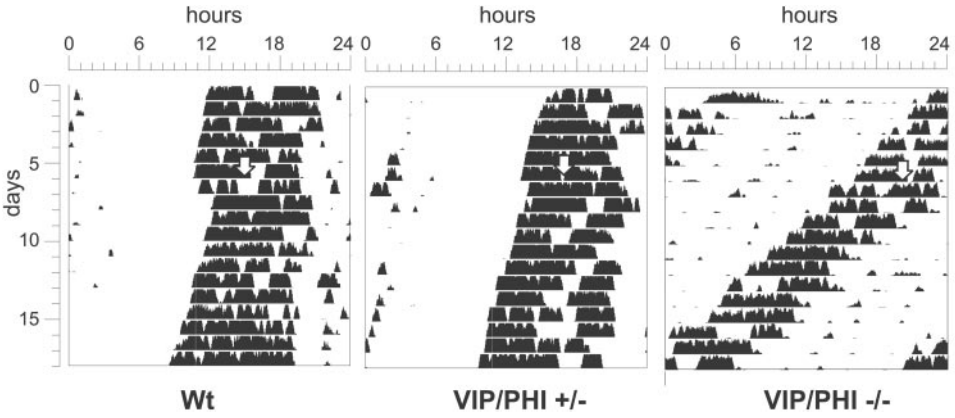

Fig. 6. Examples of light-induced phase shifts of wheel-running activity records from VIP/PHI +/+, +/−, and −/− mice. The mice were maintained in DD, and wheel-running activity was recorded. Mice were exposed to light (white light, 15 μW/cm², 10 min) at circadian time (CT) 16 at the time indicated by the white arrows. Compared with wild-type controls, the VIP/PHI +/− mice exhibited ~50% reduction in the magnitude of light-induced phase shifts, whereas the VIP/PHI −/− mice failed to exhibit a phase shift. However, the instabilities in activity onset seen in many of VIP/PHI −/− animals make measurement of phase shifts difficult.

5-min application) increased the IPSC frequency (40 ± 8%, $n = 7$, $P < 0.05$), whereas PHI (100 nM) had no significant effects (0.2 ± 2%, $n = 6$). The effects of VIP on frequency were concentration dependent (Fig. 7*B*) and long lasting, as the frequency remained elevated for at least 30 min after the end of treatment. VIP did not significantly alter the IPSC amplitudes or rise and fall times recorded in SCN neurons. Additional experiments were performed on VIP/PHI +/+ mice with a "mixed background," i.e., they were offspring (F2 generation) of C57BL/6 × 129/sv VIP −/− mice. In these mice, the mean frequency of sIPSCs recorded from the SCN during the day was 9.6 ± 2.8 events/s (mean ± SE, $n = 6$), and application of VIP (100 nM, 5 min) increased the frequency by 35 ± 8% ($n = 6$). Finally, in VIP/PHI −/− mice, VIP (100 nM) increased the frequency (48 ± 17% increase, $n = 6$) but not the amplitude of the sIPSCs. There were no significant differences in the VIP-evoked enhancement of IPSC frequency recorded from wild-type, mixed-background, or VIP/PHI −/− mice. Finally, in the presence of the VPAC receptor antagonist [Ac-Tyr[1], D-Phe[2]]- growth hormone-releasing factor (GHRF) 1–29 (100 nM), application of VIP had no stimulatory effect on IPSC frequency in VIP/PHI +/+ mice (0 ± 5% increase, $n = 8$). Together, this data suggest that VIP can activate VPAC receptors to regulate inhibitory synaptic transmission within the SCN.

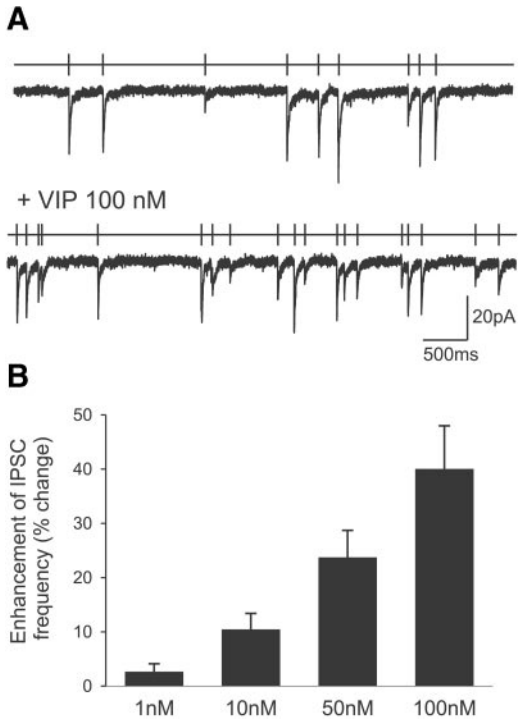

Fig. 7. Application of VIP increased the frequency of spontaneous inhibitory postsynaptic currents (sIPSCs) recorded using whole cell patch electrophysiology from SCN neurons in the C57BL/6 mouse. *A*: trace provides example of sIPSC recorded from a SCN neuron before and after treatment with VIP (100 nM, 5 min). Inhibitory postsynaptic current (IPSC) amplitude, rise time, and decay time were unaffected by VIP. Crossed lines above the traces indicate where events were detected. *B*: effects of VIP on IPSC frequency were concentration dependent. Histogram shows means ± SE; $n = 6$–8 per group.

DISCUSSION

To investigate the roles of VIP and PHI in vivo, we developed a novel mouse model in which the VIP/PHI gene was disrupted by targeted homologous recombination. Immunocytochemistry was used to confirm a lack of detectable VIP and PHI protein in the SCN of these mice. This new model system was then used to explore the role of VIP/PHI in the mammalian circadian system. In an LD cycle, the daily rhythm in wheel-running activity in the VIP/PHI-deficient mice is mostly indistinguishable from wild-type controls. The acute effects of the photic environment on locomotor activity (i.e., positive and negative masking) are apparently unaltered by the mutation. In contrast, the loss of VIP/PHI had dramatic effects on multiple aspects of the circadian system as measured by the rhythm in wheel-running activity. First and foremost, all of the VIP/PHI-deficient mice exhibited a disruption in their ability to express a coherent circadian rhythm. In the most extreme cases, some of the VIP/PHI-deficient mice (≈25%) exhibited wheel-running behavior that was arrhythmic on the circadian time scale by the end of their time in DD. The remainder of the mutant mice expressed a rhythm with a significantly shortened period that lacked coherence and statistical power because of variability in activity onset and expansion of α. When placed on a skeleton photoperiod consisting of

two light pulses per 24-h cycle, all of the VIP/PHI −/− animals exhibited two discrete activity bouts instead of the one activity bout seen in controls. Previous studies have found severe disruptions in circadian function in mice deficient in the expression of the $VPAC_2$ receptor (9, 13) that recognizes both VIP and PACAP. These $VPAC_2$ −/− mice lacked rhythmicity at the molecular, cellular, and behavioral levels. Compared with the VIP/PHI −/− mice, the loss of the receptor apparently resulted in a more severe phenotype. One potential explanation for the differences is that $VPAC_2$ receptors respond to both PACAP and VIP. Thus VIP and $VPAC_2$ −/− mice potentially yield different types of information, depending on the additional physiological interaction of PACAP with $VPAC_2$ receptors in the SCN. In any case, this difference raises the possibility that the $VPAC_2$ receptors may mediate more than just the actions of VIP and PHI. The results reported here show that the loss of VIP/PHI is sufficient to produce severe disruptions in the circadian system. Taken together, circadian studies with VIP/PHI-, $VPAC_2$- (13), and PAC1-deficient mice (11) clearly indicate that this neuropeptide family plays critical roles in the generation and regulation of circadian oscillations.

In addition, the loss of VIP/PHI appears to have altered the entrainment of the circadian oscillator to the environment. This phenotype is seen in the experiments in which animals are released into DD from an LD cycle. A wild-type mouse synchronized or entrained to a 12:12-h LD cycle will start its activity from a phase predicted from the prior LD cycle, and, for a nocturnal organism, the activity will start from a phase near the start of nocturnal activity in LD. For example, the VIP/PHI +/+ animals began their free-running rhythm within minutes of the time of lights-off in the prior LD cycle. In contrast, the VIP/PHI −/− animals started their activity ~8 h before the time of the prior lights-off. The shorter period cannot account for this large shift in activity onset. When these mice were exposed to the dark during the middle of the day (ZT 7), the endogenous drive toward activity was unmasked, as the mutant, but not wild-type, mice exhibited strong wheel-running activity. We postulate that most of this response must be due to an alteration in the processes that couple the oscillator to the environment. This argument is further supported by the altered phase angle of entrainment seen in the VIP/PHI −/− mice entrained to a single light pulse per cycle. Similarly, the $VPAC_2$ −/− mice also exhibit an extremely positive phase angle of entrainment (13). Thus our data lead us to propose that VIP and perhaps PHI are required for normal light-induced synchronization of the circadian system. This proposition is specifically supported by the observation that the VIP/PHI +/− mice exhibited ~50% reduction in the magnitude of light-induced phase shifts. The VIP/PHI −/− mice did not show any phase shift in response to short light pulses, although the variability in activity onset made this analysis difficult. In addition, previous studies have shown that VIP can mimic some of the actions of light on the SCN. Microinjection of VIP alone (25) or in combination with other peptides (2) into the SCN region can cause phase shifts of the circadian rhythm of wheel-running activity in the hamster. PHI is expressed in cells in the SCN (e.g., Refs. 24 and 29), and injections of this peptide into the SCN can cause small phase shifts in the early night (2, 25). Although distinct receptors for PHI have not been identified in mammals, this VIP-related peptide acts as a weak agonist on cloned rodent $VPAC_2$ receptors in transfected cells, albeit at concentrations 10-fold lower than VIP (15, 35). Although it is not clear whether this peptide is used as a signaling molecule, it is possible that the loss of PHI contributes to the circadian phenotype described in this study. Application of VIP also phase shifts the circadian rhythm of vasopressin release (38) and neural activity (26) measured in vitro. Finally, a recent study reports that VIP induces *mPer1* and *mPer2* gene expression during the subjective night (22). These genes are part of the basic molecular feedback loop that drives circadian oscillations in single cells and are normally regulated by light (17, 28). The normal light induction of these *mPer* genes is absent in the $VPAC_2$ −/− mice (13). Together, these observations suggest that VIP plays a significant role in coupling of the circadian oscillator to the environment.

In our view, there are two reasonable explanations for the diverse set of phenotypes observed in the VIP/PHI −/− mice. These explanations are not mutually exclusive and speak to the functional role of VIP, and perhaps PHI, in the mammalian circadian system. First, VIP and the $VPAC_2$ receptor may be required for the basic molecular oscillation that is thought to drive circadian oscillations within single cells. Experimentally, this argument is supported by the observation that the circadian oscillations in several core clock genes as well as electrical activity are lost in the $VPAC_2$ −/− mice (9, 13). Conceptually, this explanation is supported by the recent observation in *Drosophila* that the targeted expression of a modified potassium channel, and the presumed hyperpolarization of the neurons driving circadian oscillations in behavior, blocked the behavior output and also the rhythmic gene expression (23). Broadly speaking, this suggests that electrical activity at the membrane of the neuron can have a profound effect on the rhythmic patterns of gene expression and suggests a mechanism by which the loss of a signaling neuropeptide can cause deficits in rhythmic gene expression. However, it must be pointed out that most of the VIP/PHI-deficient mice still express rhythmic locomotor activity, indicating that some rhythm-generation machinery is still operational in these animals. A second possibility is that the loss of VIP/PHI alters the communication between cell populations within the SCN. Perhaps the most striking piece of experimental data supporting this hypothesis is our observation that all of the VIP/PHI −/− animals exhibited two discrete activity bouts when placed on a skeleton photoperiod consisting of two light pulses per cycle. Additional support comes from the loss of coherence and arrhythmicity seen in the locomotor activity records of VIP/PHI-deficient mice in DD. It is clear that

the application of VIP alters the firing rate of SCN neurons, with ~50% of neurons responding to VIP with a decrease of activity (26). Our electrophysiological analysis also indicates that VIP regulates inhibitory synaptic transmission within the SCN (16). It is widely accepted that most SCN neurons are GABAergic and are likely to use this transmitter to communicate with other neurons within and beyond the SCN (1, 7). Under culture conditions in which individual SCN neurons have the ability to generate circadian rhythms in firing rate, GABAergic mechanisms appear to have the capability to synchronize SCN cell populations (18, 34). Thus, by regulating inhibitory synaptic release, the loss of VIP could broadly impair communication among SCN cell populations. Certainly, a better understanding of the cellular mechanisms by which VIP regulates SCN neurons is a critical step toward the development of a mechanistic explanation for phenotype observed in VIP/PHI-deficient mice. If the deficit in these mice is primarily one impacting cellular communication, then we expect that individual neurons in the VIP/PHI −/− mice will continue to generate normal circadian oscillations, whereas deficits will emerge at the tissue level because of the weakening of coordination between the individual oscillators. While this prediction awaits future study, it may be that VIP has multiple actions within the SCN cell populations. The studies reported here clearly show that loss of VIP/PHI is sufficient to produce severe disruptions in the generation of circadian oscillations and the synchronization of these rhythms to the environment. Certainly, our data suggest that neuropeptides in the VIP family play a central role in the mammalian circadian timing system.

W. Rodriguez, J. Tam, V. Lelievre, Z. Hu, X. Liu, and J. A. Waschek were responsible for the generation of the VIP/PHI-deficient mice. J. Itri, S. Michel, and C. S. Colwell were responsible for the behavioral and electrophysiological analysis. Finally, we acknowledge J. Asai for expert assistance with the immunocytochemical analysis.

DISCLOSURES

This work was supported by National Heart, Lung, and Blood Institute Grant HL-64582 and National Institute of Neurological Disorders and Stroke Grant NS-43169 to C. S. Colwell and National Institute of Child Health and Human Development Grants HD-06576 and HD-34475 to J. A. Waschek.

REFERENCES

1. **Abrahamson EE and Moore RY.** Suprachiasmatic nucleus in the mouse: retinal innervation, intrinsic organization and efferent projections. *Brain Res* 916: 172–191, 2001.
2. **Albers HE, Liou SY, Stopa EG, and Zoeller RT.** Interaction of colocalized neuropeptides: functional significance in the circadian timing system. *J Neurosci* 11: 846–851, 1991.
3. **Berson DM, Dunn FA, and Takao M.** Phototransduction by retinal ganglion cells that set the circadian clock. *Science* 295: 1070–1073, 2002.
4. **Buijs RM, Wortel J, and Hou YX.** Colocalization of gamma-aminobutyric acid with vasopressin, vasoactive intestinal peptide, and somatostatin in the rat suprachiasmatic nucleus. *J Comp Neurol* 358: 343–352, 1995.
5. **Cagampang FR, Sheward WJ, Harmar AJ, Piggins HD, and Coen CW.** Circadian changes in the expression of vasoactive intestinal peptide 2 receptor mRNA in the rat suprachiasmatic nuclei. *Brain Res Mol Brain Res* 54: 108–112, 1998.
6. **Cambras T, Vilaplana J, Campuzano A, Canal-Corretger MM, Carulla M, and Diez-Noguera A.** Entrainment of the rat motor activity rhythm: effects of the light-dark cycle and physical exercise. *Physiol Behav* 70: 227–232, 2000.
7. **Castel M and Morris JF.** Morphological heterogeneity of the GABAergic network in the suprachiasmatic nucleus, the brain's circadian pacemaker. *J Anat* 196: 1–13, 2000.
8. **Colwell CS.** NMDA-evoked calcium transients and currents in the suprachiasmatic nucleus: gating by the circadian system. *Eur J Neurosci* 13: 1420–1428, 2001.
9. **Cutler DJ, Haraura M, Reed HE, Shen S, Sheward WJ, Morrison CF, Marston HM, Harmar AJ, and Piggins HD.** The mouse VPAC2 receptor confers suprachiasmatic nuclei cellular rhythmicity and responsiveness to vasoactive intestinal polypeptide in vitro. *Eur J Neurosci* 17: 197–204, 2003.
10. **Gillette MU.** Cellular and biochemical mechanisms underlying circadian rhythms in vertebrates. *Curr Opin Neurobiol* 7: 797–804, 1997.
11. **Hannibal J, Jamen F, Nielsen HS, Journot L, Brabet P, and Fahrenkrug J.** Dissociation between light-induced phase shift of the circadian rhythm and clock gene expression in mice lacking the pituitary adenylate cyclase activating polypeptide type 1 receptor. *J Neurosci* 21: 4883–4890, 2001.
12. **Hannibal J, Moller M, Ottersen OP, and Fahrenkrug J.** PACAP and glutamate are co-stored in the retinohypothalamic tract. *J Comp Neurol* 418: 147–55, 2000.
13. **Harmar AJ, Marston HM, Shen S, Spratt C, West KM, Sheward WJ, Morrison CF, Dorin JR, Piggins HD, Reubi JC, Kelly JS, Maywood ES, and Hastings MH.** The VPAC2 receptor is essential for circadian function in the mouse suprachiasmatic nuclei. *Cell* 109: 497–508, 2002.
14. **Hattar S, Liao HW, Takao M, Berson DM, and Yau KW.** Melanopsin-containing retinal ganglion cells: architecture, projections, and intrinsic photosensitivity. *Science* 295: 1065–1070, 2002.
15. **Inagaki N, Yoshida H, Mizuta M, Mizuno N, Fujii Y, Gonoi T, Miyazaki J, and Seino S.** Cloning and functional characterization of a third pituitary adenylate cyclase-activating polypeptide receptor subtype expressed in insulin-secreting cells. *Proc Natl Acad Sci USA* 91: 2679–2683, 1994.
16. **Itri J and Colwell CS.** Presynaptic regulation of inhibitory synaptic transmission by vasoactive intestinal peptide (VIP) in the mouse suprachiasmatic nucleus. *J Neurophyiol*. In press.
17. **King DP and Takahashi JS.** Molecular genetics of circadian rhythms in mammals. *Annu Rev Neurosci* 23: 713–742, 2000.
18. **Liu C and Reppert SM.** GABA synchronizes clock cells within the suprachiasmatic circadian clock. *Neuron* 25: 123–128, 2000.
19. **Michel S, Itri J, and Colwell CS.** Excitatory mechanisms in the suprachiasmatic nucleus: the role of AMPA/KA glutamate receptors. *J Neurophysiol* 88:817–828, 2002.
20. **Moga MM and Moore RY.** Organization of neural inputs to the suprachiasmatic nucleus in the rat. *J Comp Neurol* 389: 508–534, 1997.
21. **Mrosovsky N.** Masking: history, definitions, and measurement. *Chronobiol Int* 16: 415–429, 1999.
22. **Nielsen HS, Hannibal J, and Fahrenkrug J.** Vasoactive intestinal polypeptide induces *per1* and *per2* gene expression in the rat suprachiasmatic nucleus late at night. *Eur J Neurosci* 15: 570–574, 2002.
23. **Nitabach MN, Blau J, and Holmes TC.** Electrical silencing of *Drosophila* pacemaker neurons stops the free-running circadian clock. *Cell* 109: 485–495, 2002.
24. **Peytevin J, Aioun J, and Chambille I.** Neurons that express the AMPA receptor GluR2/3 subunits in suprachiasmatic nuclei of Syrian hamsters colocalize either vasoactive intestinal peptide, peptide histidine isoleucine or gastrin-releasing peptide. *Cell Tissue Res* 300: 345–359, 2000.
25. **Piggins HD, Antle MC, and Rusak B.** Neuropeptides phase shift the mammalian circadian pacemaker. *J Neurosci* 15: 5612–5622, 1995.
26. **Reed HE, Cutler DJ, Brown TM, Brown J, Coen CW, and Piggins HD.** Effects of vasoactive intestinal polypeptide on neurones of the rat suprachiasmatic nuclei in vitro. *J Neuroendocrinol* 14: 639–646, 2002.

27. **Reed HE, Meyer-Spasche A, Cutler DJ, Coen CW, and Piggins HD.** Vasoactive intestinal polypeptide (VIP) phase-shifts the rat suprachiasmatic nucleus clock in vitro. *Eur J Neurosci* 13: 839–843, 2001.
28. **Reppert SM and Weaver DR.** Molecular analysis of mammalian circadian rhythms. *Annu Rev Physiol* 63: 647–676, 2001.
29. **Romijn HJ, Sluiter AA, Pool CW, Wortel J, and Buijs RM.** Differences in colocalization between Fos and PHI, GRP, VIP and VP in neurons of the rat suprachiasmatic nucleus after a light stimulus during the phase delay versus the phase advance period of the night. *J Comp Neurol* 372: 1–8, 1996.
30. **Sena M, Agoston D, and Waschek J.** High conservation of upstream regulatory sequence on the mouse and human vasoactive intestinal peptide genes. *DNA Seq* 5: 25–29, 1994.
31. **Shen S, Spratt C, Sheward WJ, Kallo I, West K, Morrison CF, Coen CW, Marston HM, and Harmar AJ.** Overexpression of the human VPAC2 receptor in the suprachiasmatic nucleus alters the circadian phenotype of mice. *Proc Natl Acad Sci USA* 97: 11575–11580, 2000.
32. **Shinohara K, Funabashi T, and Kimura F.** Temporal profiles of vasoactive intestinal polypeptide precursor mRNA and its receptor mRNA in the rat suprachiasmatic nucleus. *Brain Res Mol Brain Res* 63: 262–267, 1999.
33. **Shinohara K, Tominaga K, and Inouye ST.** Phase dependent response of vasoactive intestinal polypeptide to light and darkness in the suprachiasmatic nucleus. *Neurosci Res* 33:105–110, 1999.
34. **Shirakawa T, Honma S, Katsuno Y, Oguchi H, and Honma KI.** Synchronization of circadian firing rhythms in cultured rat suprachiasmatic neurons. *Eur J Neurosci* 12: 2833–2838, 2000.
35. **Usdin TB, Bonner TI, and Mezey E.** Two receptors for vasoactive intestinal polypeptide with similar specificity and complementary distributions. *Endocrinology* 135: 2662–2680, 1994.
36. **Waschek JA, Bravo DT, Sena M, Casillas R, Rodriguez W, Nguyen T, and Colburn S.** Targeting of embryonic and postnatal autonomic and enteric neurons with a vasoactive intestinal peptide transgene. *J Neurochem* 73: 1739–1748, 1999.
37. **Waschek JA, Krajniak KG, Bravo DT, and Agoston DA.** Regulation of human and mouse vasoactive intestinal peptide genes. *Biomed Res (Tokyo) 13, Suppl* 2: 1–6, 1992.
38. **Watanabe K, Vanecek J, and Yamaoka S.** In vitro entrainment of the circadian rhythm of vasopressin-releasing cells in suprachiasmatic nucleus by vasoactive intestinal polypeptide. *Brain Res* 877: 361–366, 2000.